



Predicting the strength of European beech (*Fagus sylvatica* L.) boards using image-based local fibre direction data

Thomas Ehrhart¹ · Pedro Palma² · Mark Schubert³ · René Steiger² · Andrea Frangi¹

Received: 28 January 2021 / Accepted: 13 November 2021 / Published online: 6 December 2021
© The Author(s), under exclusive licence to Springer-Verlag GmbH Germany, part of Springer Nature 2021

Abstract

Image-based local fibre direction data, generated based on the analysis of the medullary spindle pattern, were used to improve the prediction of the tensile strength parallel to the grain of European beech (*Fagus sylvatica* L.) boards. An approach to characterise the local fibre orientations in a board using a single numerical grading parameter was further developed. This parameter was used, in combination with the dynamic modulus of elasticity, to develop a regression model providing very good predictions of the experimentally determined tensile strength parallel to the grain ($R^2 = 0.84$). Subsequently, machine-learning techniques were used to improve the strength model. Non-destructive and destructive tests were performed on ($N =$) 47 boards. A data (sub-) set ($n = 36$) was used to train different machine-learning techniques (Support-Vector Machines, Decision Tree, Random Forest, and Artificial Neural Network) using a 6-k cross-validation approach. The generalisation ability of the models was then assessed by a hold-out dataset ($n = 11$). The results showed that all machine-learning models presented good prediction accuracy (R^2 up to 0.88 and MAPE below 8%). The support-vector machine and random forest methods showed the best performance. The combination of experimental methods with machine learning allows for a more precise strength grading of timber and, thus, can contribute to a more resource-efficient use of wood and may open new and more demanding fields for high-level timber applications in structures.

Thomas Ehrhart and Pedro Palma shared joint first authorship.

✉ Pedro Palma
pedro.palma@empa.ch

¹ Institute of Structural Engineering, ETH Zürich, Stefano-Franscini-Platz 5, 8093 Zurich, Switzerland

² Structural Engineering Research Laboratory, Empa – Swiss Federal Laboratories for Materials Science and Technology, Ueberlandstrasse 129, 8600 Duebendorf, Switzerland

³ Cellulose and Wood Materials, Empa – Swiss Federal Laboratories for Materials Science and Technology, Ueberlandstrasse 129, 8600 Duebendorf, Switzerland

Introduction

Background

Timber is a material with an excellent strength–weight ratio, the possibility of being sustainably sourced, and usually perceived as aesthetically very pleasant. However, human influence on its physical and mechanical properties is generally very limited due to the natural growth, leading to a high variability in timber properties. Without taking measures to reduce the variability, large safety factors would be needed when designing timber structures, limiting the efficiency in utilising the material. For instance, during the production of glued laminated timber (GLT) or cross-laminated timber (CLT), the raw material needs to be strength graded to ensure minimum performance requirements and optimise its use. Strength grading of timber into different strength classes based on parameters obtained from non-destructive tests allows for a reduction in the material's variability and, thus, for a more efficient utilisation of the raw material. Therefore, strength grading depends mainly on the correlations between the measured (indicating) parameters and the target mechanical parameters.

State of the art

Anatomical characteristics, such as large single knots, knot clusters, bark inclusions and fibre deviations, cause the most significant reduction in the strength of timber. Regarding glued laminated timber, the tensile strength of the laminations is the key property for allocating timber boards to a certain strength class (e.g. Ehlbeck et al. 1985; Brandner and Schickhofer 2008; Fink 2014). Close to knots and in knot clusters, the tensile strength of a board is reduced due to local deviations to the mainly longitudinal fibre direction and due to the reduction in cross-sectional area available for these fibres in the presence of knots. This results in non-uniform stress distributions in these cross sections, especially in case of eccentric knots (Foley 2001). Limits regarding the knot size are provided for different grades in current strength grading standards, such as DIN 4074-1 (2012), for strength grading of coniferous sawn timber, and DIN 4074-5 (2008), for strength grading of deciduous sawn timber. For boards with fewer and smaller knots, the influence and importance of other characteristics increase. In particular, the local fibre direction becomes more important. DIN 4074-1 (2012) and DIN 4074-5 (2008) specify threshold values of this grading parameter that correspond to the various grades too. The local fibre direction also has a high influence on the strength of finger joints in beech wood laminations (Aicher et al. 2001). The detection and quantification of the fibre direction are much more complex than the determination of the size of knots and are particularly relevant to machine grading (Ridley-Ellis et al. 2016). On the one hand, the fibre direction is often difficult to detect with the naked eye; on the other hand, the fibre direction changes continuously along the length and width of a board. To overcome these problems, procedures and instruments have been developed to automatically evaluate the fibre direction (Schlotzhauer et al. 2018).

Multiple physical principles are employed to evaluate the fibre direction. Among them are the dielectric properties of wood (Baradit et al. 2006; Denzler and Weidenhiller 2015; Norimoto and Yamada 1972), the electrical field strength (Cramer and McDonald 1989; Norton et al. 1974; Steele et al. 1991), the thermal conductivity (Belkacemi et al. 2016; Daval et al. 2015; Krapez et al. 1996), and the so-called tracheid effect (Matthews et al. 1976, 1986; Metcalfe et al. 2002; Nyström 2003; Sarén et al. 2006; Simonaho et al. 2004; Soest 1997). The method based on the tracheid effect has been frequently used in descriptions and models of timber and its anatomical structure (Briggert et al. 2016; Foley, 2001; Lukacevic and Füssl 2014). The tracheid effect has been used to improve the strength grading of coniferous timber (Brännström et al. 2008; Olsson et al. 2013; Olsson and Oscarsson 2017; Viguier et al. 2015, 2017). More recently, it has also been applied successfully to fibre orientation measurements on hardwoods (Besseau et al. 2020), on beech veneers to estimate the modulus of elasticity of LVL (Viguier et al. 2018), and to strength grading of oak (Olsson et al. 2018).

The vast majority of the mentioned investigations focussed on coniferous timber species, mainly Norway spruce (*Picea abies* (L.) Karst.). For European beech (*Fagus sylvatica* L.) timber, significantly fewer studies are available. In Switzerland, Germany, and Austria, European beech amounts to 18, 15, and 10% of the total forest stock, respectively, corresponding to shares between 50 and 80% of the hardwood stock in these countries (FOEN 2018; Sauter and Breinig 2016). European beech timber is also among the European native species with the highest strength and stiffness properties. Compared to timber from coniferous trees, European beech timber exhibits significantly fewer knots and knot-free boards predominate in high-strength classes. Consequently, the strength grading parameter fibre direction is of utmost importance.

Ehrhart et al. (2018a) presented a non-contact method for the identification, quantification, and documentation of the fibre direction in European beech timber based on the analysis of the medullary rays. Making use of image-analysis techniques, the spindle pattern formed by the medullary rays was used to predict the fibre direction in European beech boards. Curti et al. (2018) adapted this method to investigate the effect of fibre direction on cutting forces and chip geometry during machining of beech timber in the fibre-saturated state.

To further increase the reliability and utilisation efficiency of timber in general, improved machine grading procedures are required to measure various grading parameters at high speed, with greater accuracy and precision. In general, the correlation between the measured grading parameters and the structural properties is performed using simple linear or multilinear correlations (Ehlbeck et al. 1985; Fink 2014), neglecting that the structure of timber is complex and that these correlations are often nonlinear. Machine-learning techniques are particularly suited to overcome challenges related to finding patterns in complex systems. These data-driven approaches are able to identify hidden patterns in data of different type and create classification and predictive models (Fathi et al. 2020; Schubert and Kläusler 2020). Combining machine-learning techniques with non-destructive optical and digital image analysis methods is therefore a promising strategy for grading high-strength timber boards with few obvious visual defects. These advanced grading techniques

can be further complemented with mechanical constitutive models, which establish the relation between material parameters and external loads (e.g. Sarnaghi and van de Kuilen 2019), leading to hybrid strength grading approaches.

Objective, scope, and overview

The objective of this study was to develop a model to improve the prediction of the tensile strength of European beech (*Fagus sylvatica* L.) boards without obvious visual defects. The developed model considers the measured dynamic modulus of elasticity and new information on the fibre direction, obtained through a non-destructive and non-contact method developed by Ehrhart et al. (2018a). Different machine-learning techniques are applied, and their potential for maximising the prediction quality of the models is evaluated.

Materials and methods

Overview

This study was based on 47 flat sawn planed beech boards supplied by four Swiss sawmills. The dimension of the boards was $l_b \times w_b \times t_b = 3000 \times 160 \times 25 \text{ mm}^3$. The thickness of the beech laminations $t_b = 25 \text{ mm}$ is significantly smaller than usual thicknesses of softwood laminations (up to 40 mm), but this is due to delamination problems arising when beech laminations thicker than 30 mm are used (Ohnesorge et al. 2010) for glulam production. The average moisture content of the boards at the time of testing was $\omega = 8 \pm 2\%$. This moisture content corresponds to an environment with 24 °C and 35% relative humidity, which is not uncommon in offices and residential buildings and also corresponded to the expected environmental conditions in the laboratories where the tests were performed. Since the focus of this study was on improving the grading of high strength boards, only boards free of knots, bark inclusions and other obvious structural characteristics affecting the tensile strength parallel to the grain were considered. The wide faces of the boards were mostly parallel to the longitudinal-tangential plane of the wood. In such knot-free boards, the influence of fibre orientation on the tensile strength becomes more important. Ehrhart et al. (2018a) have shown that the medullary ray spindle pattern, which is clearly visible on the face sides, can be used to assess the local fibre orientation. About 75% of the 47 boards were comprehensively photographed, documented, and tested to failure in tension parallel to the grain by Ehrhart et al. (2016b). The other 25% of the boards were analysed, and the density, the dynamic MOE, the surface photographs and the experimental tensile strength were documented by Jungo (2016). The data sets collected by Ehrhart et al. (2016a) and Jungo (2016) were combined and subsequently randomly split into two data sets: a training or calibration data set (used to fit models) and a test data set (used to evaluate the models). The training data set consisted of 36 boards (77%) and the test data set of 11 boards (23%). The total number of boards used in this study is limited, but was shown to be adequate to

assess the ability of the proposed method of using image-based local fibre direction data to very significantly improve the prediction of the tensile strength of European beech boards.

2.2 Strength grading parameters measured using non-destructive methods

Density and dynamic modulus of elasticity

The devices *Brookhuis MTG Timber Grader* and *Microtec ViScan* were used to determine the density and the dynamic modulus of elasticity of the beech boards (Ehrhart (2019) showed that the two systems provide almost identical results). The dynamic modulus of elasticity E_{dyn} is calculated using Eq. (1), based on the first longitudinal eigenfrequency f_e , the density ρ and the length l_b of the board.

$$E_{\text{dyn}} = 4 \cdot f_e^2 \cdot l_b^2 \cdot \rho \quad (1)$$

The statistical parameters of the dynamic modulus of elasticity and density are summarised in Table 1 for both the training ($n=36$) and the test ($n=11$) data sets. The range of density is wider for the training data set (647–817 kg/m³) than for the test data set (671–759 kg/m³). However, the mean values of density at a moisture content of $\omega=8\pm 2\%$ ($\rho_{8,\text{mean}}$) and the coefficients of variation (cov) of both data sets agree well (726 and 710 kg/m³ and 0.05 and 0.04, respectively). Similar values of densities of European beech are reported by Frühwald and Schickhofer (2005), Frese (2006), Hübner (2013), and Westermayr et al. (2018).

Table 1 Statistical parameters for the density ρ , dynamic modulus of elasticity E_{dyn} , static modulus of elasticity $E_{t,0}$ and tensile strength parallel to the grain $f_{t,0}$ of the training and test data sets ($\omega=8\pm 2\%$)

	Parameter	Symbol	Unit	n^* [-]	Min	Mean	Max	Cov [-]
All boards	Density	ρ	kg/m ³	47	647	722	817	0.05
	Dynamic modulus of elasticity (MOE)	E_{dyn}	MPa		12,805	16,466	23,371	0.13
	Static MOE	$E_{t,0}$	MPa		12,102	15,479	20,457	0.12
	Tensile strength	$f_{t,0}$	MPa		42.2	88.5	132	0.25
Training data set**	Density	ρ	kg/m ³	36	647	726	817	0.05
	Dynamic MOE	E_{dyn}	MPa		12,805	16,520	23,371	0.14
	Static MOE	$E_{t,0}$	MPa		12,102	15,428	20,457	0.11
	Tensile strength	$f_{t,0}$	MPa		42.2	85.4	132	0.25
Test data set**	Density	ρ	kg/m ³	11	671	710	759	0.04
	Dynamic MOE	E_{dyn}	MPa		13,613	16,291	20,791	0.14
	Static MOE	$E_{t,0}$	MPa		12,288	15,646	18,985	0.13
	Tensile strength	$f_{t,0}$	MPa		49.5	90.4	119	0.26

*Number of boards

**The data were split into two data sets: one for training (i.e. calibrating) the models and one for testing the fitted models

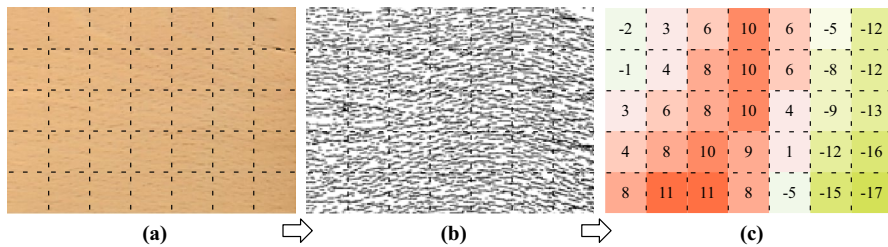


Fig. 1 Non-contact determination of the fibre direction: based on a photograph (a), the medullary ray spindles are isolated (b), and their coordinates and geometrical properties are documented. Post-processing of the resulting data allows generating discretised fields of fibre direction, e.g. average local angle between the fibre directions and the longitudinal direction of the boards (c)

The range of the dynamic modulus of elasticity is also wider for the training (12,805–23,371 MPa) than for the test data set (13,613–20,791 MPa), and the mean value of the training data set is slightly higher than that of the test data set (16,520 and 16,291 MPa, respectively). Frese (2006) reported a range of 9656–20,613 MPa and a mean value of 14,506 MPa.

Local fibre direction

The local fibre direction was identified, quantified, and documented using the non-destructive and non-contact method developed by Ehrhart et al. (2018a). This method assumes that the medullary rays and the annual rings form corridors, along which the wood fibres run and, thus, are a proxy for the fibre direction. Due to the low shear strength of European beech wood in the longitudinal-radial plane (Ashby et al. 1985), the spindles formed by the medullary rays were found to be an excellent indicator for the critical fibre direction, i.e. the fracture path developing in destructive tension tests.

The two opposite face sides of the middle 2000 mm (=tested free-length of the boards in the tension tests, see Subsection [Tensile strength parallel to the grain measured in tension tests to failure](#)) of the 3000 mm long boards were documented by taking four consecutive photographs of 500-mm-long segments. Hence, eight photographs were taken of each board. Figure 1a shows a part of one of the resulting digital photographs. Subsequently, these digital images were batch-processed to isolate and identify the medullary ray spindles using the programme *Adobe Photoshop 2020*. The steps of this pre-processing were: (i) smart sharpening (amount: 500%, radius: 7.5 pixels); (ii) convert mode (to grayscale); (iii) apply a cut-out filter (levels=4, edge simplicity=1; edge fidelity=3); set a threshold (level: 75). Each file covers a board length of 500 mm, and the resulting PNG-files have an approximate size of 100 kB (the original size of the photograph was approximately 5 MB). The black-and-white image showing the isolated medullary ray spindles of the photograph in Fig. 1a is shown in Fig. 1b.

The black-and-white PNG images were analysed using the programme *ImageJ* (Image Processing and Analysis in Java) (Schindelin et al. 2012). By applying a

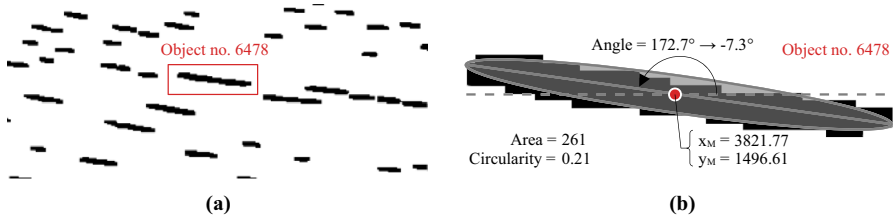


Fig. 2 Detail image of board no. 1004, segment no. 4, after isolation of the medullary ray spindles (a). As an example, information on the coordinates, the area, the circularity, and the angle of object no. 6478 is shown (b)

threshold, the medullary ray spindles were identified as objects. (An example based on an image of segment no. 4 of board no. 1004 is shown in Fig. 2a.) Subsequently, a list of the properties of all objects was generated, including: coordinates x_M and y_M of the centre of mass (in pixels); area A (in pixels); circularity c (calculated using Eq. (2), in which P is the perimeter of the object in pixels); and angle α between the major axis of an ellipse fitted to the object and the longitudinal direction of the board (in degrees). The angle α was measured in counter-clockwise direction; objects with angles above 90° were considered as having negative orientations, i.e. $\alpha = \alpha_{\text{measured}} - 180$ (Fig. 2b).

$$c = 4 \cdot \pi \cdot \frac{A}{P^2} \quad (2)$$

Only objects that represent medullary ray spindles should be considered in the analysis of the field of fibre direction. Thus, objects resulting from dirt, markings or other sources were removed by filtering the resulting object list. The filtering criteria to define valid objects were: object area A between 50 and 500 pixels (approximately 0.45 to 4.50 mm^2); circularity c between 0.02 and 0.60 and; absolute orientation α below 45° . Fields of local fibre direction were then obtained by discretising the boards into surface elements with a size of ($e \times e =$) $20 \times 20 \text{ mm}^2$ and calculating the average fibre direction in each element taking into account the results for both face sides. This element size was chosen as a compromise between enough resolution to reliably detect fibre orientation and avoiding "empty" grid elements, for which no fibre orientation could be determined. If less than five elements were present in an element, no fibre direction was calculated. Figure 1c presents the resulting field of fibre direction for the segment shown in Fig. 1a and b.

Tensile strength parallel to the grain measured in tension tests to failure

Test set-up

The tensile strength parallel to the grain of the European beech boards was determined in accordance with EN 408 (2012), using a *Gehzu 850* horizontal testing machine (Fig. 3). The boards had a total length $l_b = 3000 \text{ mm}$, but the

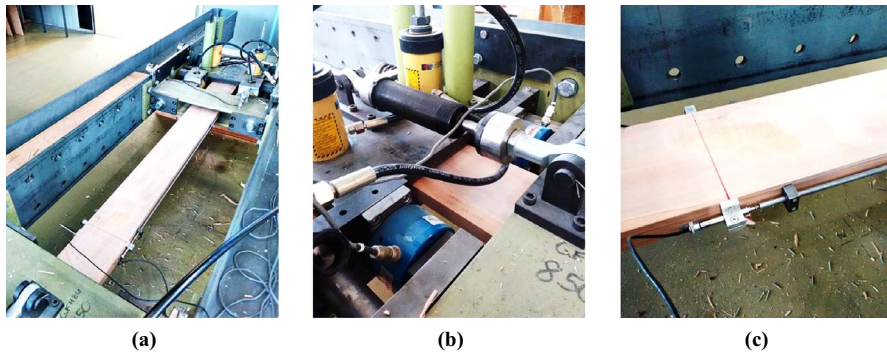


Fig. 3 Tensile testing machine *Gehzu 850*, used to determine the tensile strength parallel to the grain $f_{t,0}$ (a). Vertical hydraulic jacks that apply the clamping pressure and horizontal load cells to measure the applied tensile force (b). Displacement transducers on the edge faces, used to determine the static modulus of elasticity parallel to the grain $E_{t,0}$ (c)

free testing-length between the clamps (Fig. 3b) was $l_{\text{test}} = 2060$ mm, which was very approximately the part of the boards for which the local fibre direction was analysed (see Subsection [Local fibre direction](#)). In addition to the tensile strength parallel to the grain $f_{t,0}$, also the static modulus of elasticity parallel to the grain $E_{t,0}$ was determined in accordance with EN 408 (2012), based on measurements performed using linear variable differential transformers (LVDT) attached to both edge faces of the boards (Fig. 3c).

Test results

The statistical parameters of the tensile strength and static MOE parallel to the grain are summarised in Table 1 for the training ($n=36$) and the test ($n=11$) data sets. The range of tensile strength is slightly wider for the training data set (42.2–132 MPa; $\text{cov}=0.25$) compared to the test data set (49.5–119 MPa; $\text{cov}=0.26$). The mean value of tensile strength is about 6% lower in the training data set ($f_{t,0,\text{mean}} = 85.4$ MPa) compared to the test data set ($f_{t,0,\text{mean}} = 90.4$ MPa). Similarly, a wider range but a slightly lower mean value of the static MOE was found for the training data set ($E_{t,0,\text{mean}} = 15,428$ MPa) compared to the test data set ($E_{t,0,\text{mean}} = 15,646$ MPa).

The results of previous tensile testing campaigns on European beech boards are summarised in Table 2. The tensile strengths were between 4.3 and 142 MPa (Blaß et al. 2005; Ehrhart 2019; Frühwald and Schickhofer 2005; Glos and Lederer 2000; Plos et al. 2018; and Weidenhiller et al. 2019). Since only flat sawn boards free of knots were investigated in this study, the variation of results is significantly lower. No strength values below 40 MPa were observed. Nevertheless, the maximum values in the data sets are close to those reported in other studies (Table 2).

Table 2 Tensile strength parallel to the grain of European beech boards reported in other studies

Study	Remark	Tensile strength parallel to the grain [MPa]				
		<i>n</i> * [-]	Min	Mean	Max	Cov [-]
Glos and Lederer (2000)	–	219	11.3	48.7	117	0.46
Frühwald and Schickhofer (2005)	–	112	16.7	62.3	115	0.40
Blaß et al. (2005)	–	354	–	68.1	–	0.50
Plos et al. (2018)	–	191	19.1	72.1	142	0.38
Weidenhiller et al. (2019)	Training/test data sets	21/20	–	58.7/51.3	–	0.46/0.55
Ehrhart (2019)	All boards	294	4.3	63.4	132	0.65
	tKAR ≤ 0.05	170	26.1	78.2	132	0.29
This study	tKAR = 0	47	42.2	86.6	132	0.25
	(only boards free of knots were used)					

*Number of tests

Failure patterns

As described in Ehrhart et al. (2018a), the dominating failure mode was shear failure along the spindles formed by the medullary rays. As an example of a board with the spindles formed by the medullary rays running mostly parallel to the x-axis, i.e. the longitudinal axis of the board, a segment of board no. 3002 is shown in Fig. 4a. The objects identified in this board segment are shown in Fig. 4b, where the almost horizontal orientation of the spindles is even clearer. The stain at the bottom part of the image is not considered in the calculation of the fibre direction matrix due to its circularity (> 0.6) and the orientation of the main axis of the fitted ellipse ($> 45^\circ$) (see filtering criteria in Subsection Local fibre direction). Failure cracks created in the tension tests are shown in Fig. 4c. It can be seen that these cracks run mostly parallel to the x-axis, meaning that the fibres are quite straight ($\alpha \approx 0$). Due to the small fibre inclination, a relatively high tensile strength of $f_{t,\text{experimental}} = 112$ MPa was observed with board no. 3002.

As an example of a board with a higher fibre inclination, a segment of board no. 2058 is shown in Fig. 5. Both in the original image (Fig. 5a) and the image showing the objects (Fig. 5b), a negative inclination of the spindles ($\alpha \approx -15^\circ$) is clearly seen. The actual fibre direction, revealed by the failure pattern shown in Fig. 5c, agrees well with this observation. A significantly lower tensile strength of $f_{t,0,\text{experimental}} = 42$ MPa was observed in the tensile test.

Numerical methods

Data-fitting methods

The regression parameters were calibrated by minimising the residual sum of squares (RSS) between the estimated and the experimentally determined tensile strengths. This was done using the generalised reduced gradient (GRG) nonlinear

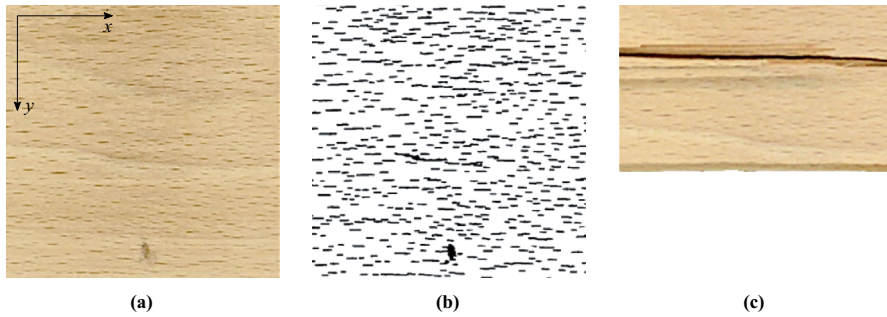


Fig. 4 Detail image of a segment of board no. 3002, the spindles formed by the medullary rays running mostly parallel to the longitudinal axis of the board (a), identified objects (b) and fracture path in the same segment (c). This board exhibited a tensile strength of 112 MPa in the tensile test to failure

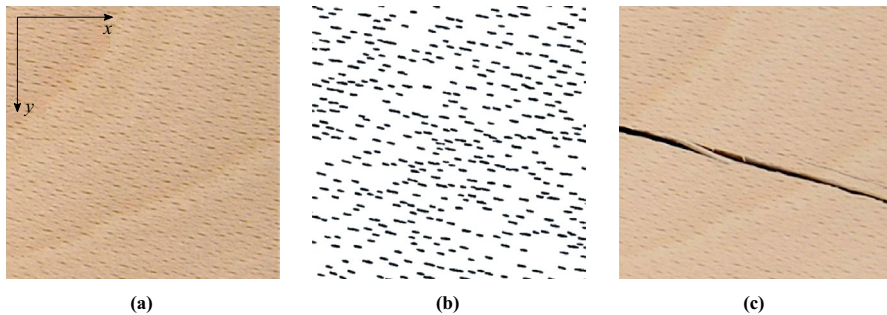


Fig. 5 Detail image of a segment of board no. 2058, with the spindles formed by the medullary rays running mostly at an angle of 15° to the longitudinal axis of the board (a), identified objects (b) and fracture path in the same segment (c). This board exhibited a tensile strength of 42 MPa in the tensile test to failure

solver implemented in MS Excel 2016. Only the training dataset (36 boards) was used in the model calibration.

Machine-learning techniques

The main objective of using machine-learning techniques is to properly adjust important hyperparameters of the algorithms and to avoid overfitting, in order to achieve a good generalisation with respect to the unseen test data (Mansfield et al. 2007). Thus, the choice of a proper experimental methodology is crucial. Therefore, as mentioned before, the data set ($N=47$) was divided in: a training data set ($n=36$) and a test data set ($n=11$). The training data set was used to identify and adjust important model hyperparameters by applying a ($k=$) sixfold cross-validation approach (Kohavi 1995). Cross-validation is a resampling procedure used to effectively evaluate machine-learning models on a limited data set (Kohavi 1995). In the process of cross-validation, one part of the training data set ($n=36$) was set as the

validation data set, while the remaining $k-1=5$ parts were used as the training data set.

After training the machine-learning algorithms using the cross-validation method, the generalisation ability was assessed with the test data set (hold-out evaluation) based on the accuracy measures: coefficient of determination (R^2); root mean square error (RMSE); and mean absolute percentage error (MAPE). The results from this evaluation serve as a quality measure (generalisation ability) for these models. Typical MAPE values for performance evaluation are categorised as follows (Lewis 1982): $\text{MAPE} \leq 10\%$ corresponds to a ‘high accuracy prediction’; $10\% < \text{MAPE} \leq 20\%$ corresponds to a ‘good prediction’; and $20 < \text{MAPE} \leq 50\%$ corresponds to a ‘reasonable prediction’. A MAPE above 50% indicates an ‘inaccurate prediction’. The input parameters for the machine-learning techniques were the same that were used in the developed physically based model.

Deep learning approaches, for example convolutional neural networks, would be particularly suited to predict the tensile strength based solely on images of the boards, but require extremely large data sets and are computationally intensive. Therefore, shallow machine-learning algorithms were used instead. Shallow algorithms require the data to be described by pre-defined features, which in this case are the grading parameters and the local fibre direction.

The machine-learning techniques applied in this study were *Support-Vector Machines* (e.g. Vapnik 1995), *Decision Trees* (e.g. Kotsiantis 2013), *Random Forest* (e.g. Breiman 2001), and *Artificial Neural Network* (e.g. Hinton and Salakhutdinov 2006).

Introduced by Vapnik (1995), *Support-Vector Machines* are supervised learning models for classification and regression. Since support-vector machine regression relies on kernel functions, it is considered a nonparametric technique. In this study, the scaling factor, i.e. the kernel scale, and the cost function were optimised using sequential minimal optimisation (SMO). *Decision Trees* build regression or classification models in the form of a tree structure (Kotsiantis 2013). Thereby, the data are split into at least two homogeneous sets (also called sub-populations) based on the most significant features of the input variables. An associated decision tree, featuring decision nodes and leaf nodes, is incrementally developed. Decision trees are precursors to Random Forests (Kotsiantis 2013). Operated by constructing a multitude of decision trees, a *Random Forest* is an ensemble learning method for (e.g.) classification and regression. Thereby, each tree is generated using a random variable subset from the candidate’s predictor variables and a random subset of data, generated by means of a bootstrap (Breiman 2001). *Artificial Neural Networks* comprise three functional parts (Hinton and Salakhutdinov 2006): (i) input layer; (ii) hidden layers; and (iii) an output layer. The hidden part can consist of many layers that enable multi-level and nonlinear operations (Hinton and Salakhutdinov 2006). The interconnections between nodes, the parameters that represent the strengths of the interconnections (weights), and the activation function, which is a nonlinear function that converts the weighted sum of the input signals to output at each node, are important features for the performance of the network and are adjusted through learning (LeCun et al. 2015). The learning process for updating weights is called “training”, which occurs in an iterative way. During each optimisation step, the

weights are adjusted in order to reduce the difference between the prediction and the measured activity (Hinton and Salakhutdinov 2006).

All algorithms were programmed in MATLAB R2018b (using the statistics and machine-learning toolbox). The hyperparameters of the Support-Vector Machines, Decision Trees, and Random Forests were optimised using Bayesian optimisation (Snoek et al. 2012). The optimal configuration, i.e. the decision about the type of training algorithm, learning rate, activation function (e.g. radial basis, tanh, ReLU) and number of layers and neurons per layer for the artificial neural network, was obtained by a trial and error approach until no further improvement could be achieved. A detailed mathematical description of the algorithms has been presented by Bishop (2006).

Development and evaluation of strength models

Overview

This study focussed on grading high-strength European beech boards free of knots. Thus, knot-related parameters, such as the single knot (DEB) and the knot cluster (DAB) parameter, or the knot area ratio (KAR) and the total knot area ratio (tKAR), could not be used in the models to estimate the tensile strength.

The potential of using the board density (ρ) and the dynamic modulus of elasticity (E_{dyn}) as grading parameters for the tensile strength parallel to the grain ($f_{t,0}$) of beech boards was investigated in several studies (Glos and Lederer 2000; Frühwald et al. 2003; Frühwald and Schickhofer 2005; Plos et al. 2018; Weidenhiller et al. 2019; Ehrhart, 2019). The reported coefficients of determination between the density and the tensile strength parallel to the grain, i.e. $R^2(\rho, f_{t,0})$, were consistently very low ($R^2 < 0.20$) (Table 3). Low coefficients of determination of $R^2 = 0.06$ were also found in the present study (Fig. 6a).

The coefficients of determination for a linear correlation between the dynamic MOE and the tensile strength parallel to the grain reported in the literature are much more diverse (Table 3). While Ehrhart (2019), Frühwald et al. (2003), and Frühwald and Schickhofer (2005) reported relatively low coefficients of determination (R^2 between 0.19 and 0.27), Weidenhiller et al. (2019) observed much higher coefficients of determination ($R^2 \approx 0.60$). In this study, a coefficient of determination between the dynamic MOE and the tensile strength parallel to the grain, i.e. $R^2(E_{\text{dyn}}, f_{t,0})$, of 0.48 (Fig. 6b) was found.

Sub-model to estimate the minimum local tensile strength of a board

As described above, the fibre orientation within a board is not constant. It changes continuously both along the longitudinal as well as along the transverse axis of a board. Generally, the tensile strength is locally reduced in areas with high fibre inclination. However, not only the tensile strength but also the static MOE is smaller for elements with high fibre inclination. Consequently, the stresses in

Table 3 Coefficients of determination R^2 between the potential strength grading parameters density (ρ) and dynamic MOE (E_{dyn}) and the target parameter tensile strength parallel to the grain ($f_{t,0}$) reported in previous studies (listed in the first column of the table) and found for the data training and test sets used in the present study

	Remark	n [-]	$R^2(\rho, f_{t,0})$	$R^2(E_{\text{dyn}}, f_{t,0})$
Glos and Lederer (2000)	–	219	0.02	–
Frühwald et al. (2003)	–	70	0.17	0.19
Frühwald and Schickhofer (2005)	*	202	0.03	0.26
Plos et al. (2018)	–	191	0.05	–
Weidenhiller et al. (2019)	Training/test data	21/20	–	0.62/0.57
Ehrhart (2019)	All boards	294	0.00	0.27
	tKAR ≤ 0.05	170	0.03	0.10
Present study	All boards	47	0.06	0.48
	Training data set**	36	0.07	0.48
	Test data set**	11	0.10	0.53

*Global coefficients of determination for three hardwood species (European beech (*Fagus sylvatica* L.), oak (*Quercus robur* L.), and ash (*Fraxinus excelsior* L.))

**For training and testing of the model, the data were split into two data sets

a cross section are distributed depending on the stiffnesses of its elements and failure will not necessarily occur in the element with the highest fibre inclination. To take this into account, a sub-model to calculate the minimum local tensile strength of a board $\min(f_{t,ij})$ is implemented. A preliminary study based on this approach was presented by Ehrhart et al. (2018b). The minimum local tensile strength corresponds to the external stress that leads to the failure of the first element.

For calculating $\min(f_{t,ij})$, the local fibre orientation matrices (see Subsection **Local fibre direction**) are taken into account. Constant strain across each cross section is assumed, i.e. the stresses within a cross section are distributed according to the local static MOE of each element in the cross section. The local MOE used herein ($E_{t,ij}$) is calculated based on the local fibre direction α_{ij} of each element (Fig. 7a) using the Hankinson model (Eq. 3) (Hankinson 1921). The resulting matrix of $E_{t,ij}$ has a size of m ($=w_b/e = 160 \text{ mm}/20 \text{ mm} = 8$) $\times n$ ($=l_{\text{relevant}}/e = 2000 \text{ mm}/20 \text{ mm} = 100$).

In Eq. (3), the local fibre direction (α_{ij}), the reference static MOE parallel ($E_{t,0,\text{ref}}$) and perpendicular to the grain ($E_{t,90,\text{ref}}$) as well as the exponent (a) are considered. Subsequently, the average MOE of each cross section ($E_{t,i}$) was calculated. The exponent (a) was calibrated through a data-fitting procedure on the training data set (see Subsection **Calibration and testing of the model**).

$$E_{t,ij} = \frac{E_{t,0,\text{ref}} \cdot E_{t,90,\text{ref}}}{E_{t,0,\text{ref}} \cdot \sin^a(\alpha_{ij}) + E_{t,90,\text{ref}} \cdot \cos^a(\alpha_{ij})} \quad (3)$$

The matrix of local tensile strengths $f_{t,ij}$ (Fig. 1c), i.e. the external stress that would cause failure in the element e_{ij} , was calculated considering the local fibre direction α_{ij} , the local stiffness $E_{t,ij}$ and the mean stiffness of the cross section i using Eq. (4). The

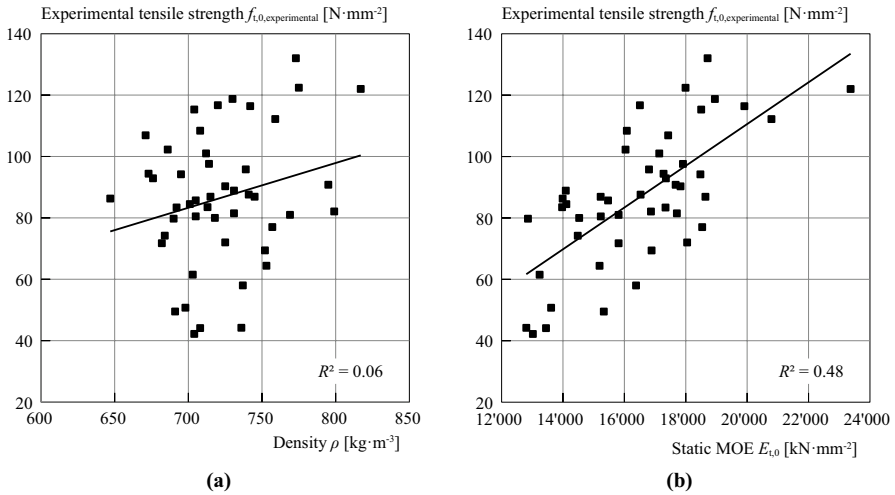


Fig. 6 Correlation of potential grading parameters density ($R^2=0.06$) (a) and dynamic modulus of elasticity ($R^2=0.48$) (b) with the target parameter tensile strength parallel to the grain ($f_{t,0}$)

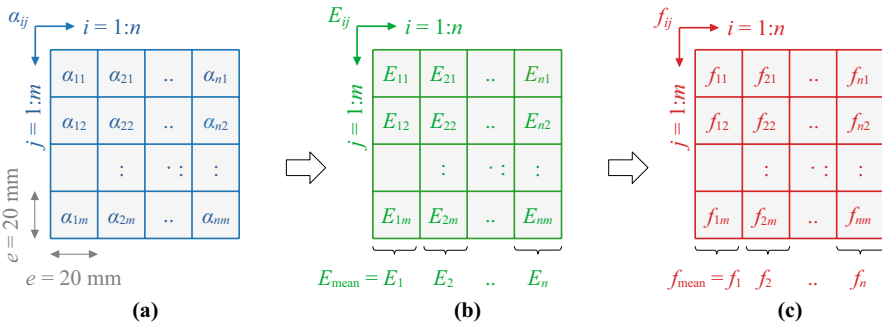


Fig. 7 Discretisation of the boards into elements ij of $e \times e = 20 \text{ mm} \times 20 \text{ mm}$. For each element, the fibre direction (a), the estimated local static modulus of elasticity $E_{t,ij}$ (b), and the estimated local tensile strength $f_{t,ij}$ (c) are determined

reference tensile strength parallel ($f_{t,0,ref}$) and perpendicular to the grain ($f_{t,90,ref}$) were chosen according to Wagenführ (2006). The calibration parameter b was determined through a data-fitting procedure on the training data set (see Subsection Calibration and testing of the model).

$$f_{t,ij} = \frac{f_{t,0,ref} \cdot f_{t,90,ref}}{f_{t,0,ref} \cdot \sin^b(\alpha_{ij}) + f_{t,90,ref} \cdot \cos^b(\alpha_{ij})} \cdot \frac{E_{t,ij}}{E_{t,i}} \tag{4}$$

In the modelling of the tensile strength ($f_{t,estimated}$), the grading parameter E_{dyn} and the grading parameter $\min(f_{t,ij})$ are taken into account. The latter one allows considering the influence of the local fibre orientation. In accordance with previous studies

(Frühwald and Schickhofer 2005; Blaß et al. 2005; Plos et al. 2018), no significant influence of the density on the tensile strength could be determined. Hence, this grading parameter is not considered in the developed model.

Sub-model to estimate the tensile strength parallel to the grain of a board

The model to estimate the tensile strength parallel to the grain of a board is based on two independent variables E_{dyn} and $\min(f_{t,ij})$. It has been shown that the dynamic modulus of elasticity E_{dyn} exhibits a medium linear correlation with the tensile strength ($R^2(X_1, \ln(f_{t,0})) = 0.48$; Fig. 6b) (correlation categorisation based on the JCSS Probabilistic Model Code (JCSS 2006): $0.8 \leftrightarrow$ high correlation, $0.6 \leftrightarrow$ medium correlation, $0.4 \leftrightarrow$ low correlation, $0.2 \leftrightarrow$ very low correlation). The independent variable $\min(f_{t,ij})$ represents the minimum of the estimated local tensile strengths of each cross section and is related to the local fibre orientation as described in Subsection [Sub-model to estimate the minimum local tensile strength of a board](#) and Fig. 7. The model assumes a multilinear correlation between the variables E_{dyn} and $\min(f_{t,ij})$ and the logarithm of the estimated tensile strength ($f_{t,\text{estimated}}$) and includes three calibration parameters (C_i) (Eq. 5).

$$\ln(f_{t,0,\text{estimated}}) = C_0 + C_1 \cdot E_{\text{dyn}} + C_2 \cdot \min(f_{t,ij}) \quad (5a)$$

$$f_{t,0,\text{estimated}} = e^{(C_0 + C_1 \cdot E_{\text{dyn}} + C_2 \cdot \min(f_{t,ij}))} \quad (5b)$$

$$f_{t,ij} = \frac{f_{t,0,\text{ref}} \cdot f_{t,90,\text{ref}}}{f_{t,0,\text{ref}} \cdot \sin^b(\alpha_{ij}) + f_{t,90,\text{ref}} \cdot \cos^b(\alpha_{ij})} \cdot \frac{\frac{E_{t,0,\text{ref}}}{E_{t,90,\text{ref}}}}{\frac{E_{t,0,\text{ref}}}{E_{t,90,\text{ref}}} \cdot \sin^a(\alpha_{ij}) + \cos^a(\alpha_{ij})} \cdot \frac{1}{m} \cdot \sum_{j=1}^m \left(\frac{\frac{E_{t,0,\text{ref}}}{E_{t,90,\text{ref}}}}{\frac{E_{t,0,\text{ref}}}{E_{t,90,\text{ref}}} \cdot \sin^a(\alpha_{ij}) + \cos^a(\alpha_{ij})} \right) \quad (6)$$

Calibration and testing of the model

The model to estimate the tensile strength of a board, resulting from combining the sub-models described in the previous subsections, is presented in Eqs. (5) and (6). Thereby, E_{dyn} is the measured dynamic MOE (see Subsection [Sub-model to estimate the tensile strength parallel to the grain of a board](#)), α_{ij} is the computed local fibre orientation, and m is the number of cross sections in the considered discretisation of the board (see Subsection [Sub-model to estimate the minimum local tensile strength of a board](#)). The calibration parameters of the model are the exponents a and b (model to estimate the minimum local tensile strength of a board, Subsection [Sub-model to estimate the minimum local tensile strength of a board](#)) and C_0 , C_1 , and C_2 (model to estimate the tensile strength of a board, Subsection [Sub-model to estimate the tensile strength parallel to the grain of a board](#)). To ensure that the

calibration parameters remain within reasonable values, i.e. that they make physical sense, the threshold values presented in Table 4 were enforced during the calibration procedure.

Since it is not the actual value but the ratio between the two parameters that has an influence on the stress distribution in the cross section, the moduli of elasticity parallel and perpendicular to the grain were combined in a single parameter, which was assumed to be $(E_{t,0,ref}/E_{t,90,ref}) = 30$ (Wagenführ, 2006). The reference tensile strength parallel to the grain ($f_{t,0,ref} = 180$ MPa) and the reference tensile strength perpendicular to the grain ($f_{t,90,ref} = 7$ MPa) were chosen according to Wagenführ (2006).

The calibration parameters were determined by minimising the residual sum of squares (RSS) between the estimated ($f_{t,0,estimated}$) and the experimentally determined tensile strengths ($f_{t,0,experimental}$) and are presented in Table 4. Only the training data set ($n = 36$) was considered in this procedure. The other 11 boards remained “unseen”. Equation (7) results from this procedure. It can be used to estimate the tensile strength of a board based on the dynamic MOE (E_{dyn}), the minimum local tensile strength $\min(f_{t,ij})$, computed based on the local fibre direction (α_{ij}), and an error term ε . The independent variable $\min(f_{t,ij})$ alone, which is only based on the local fibre direction α_{ij} , shows a medium–high linear correlation with the logarithmic value of tensile strength $\ln(f_t)$ ($R^2 = 0.65$).

$$\ln(f_{t,0,estimated}) = 1.91 + 5.06 \cdot 10^{-5} \cdot E_{dyn} + 1.21 \cdot 10^{-2} \cdot \min(f_{t,ij}) + \varepsilon \quad (7)$$

Figure 8 summarises all process steps: based on photographs of the board sections (Fig. 8a), the medullary ray spindles were identified (Fig. 8b), and the field of fibre direction was generated (Fig. 8c). The dynamic MOE (constant along the board) and the minimum local tensile strength of each cross sections i $\min(f_{t,i})$ are shown in Fig. 8d. Such information on the tensile strength for each cross section/along the board’s axis could be especially of importance for choosing the location of finger joints during fabrication. However, for the estimation of the tensile strength parallel to the grain of the board $f_{t,0,estimated}$, the lowest local tensile strength in the entire board $\min(f_{t,ij})$ is considered in Eq. (7).

In Fig. 9a, the tensile strength predicted by the developed model ($f_{t,0,estimated}$) is compared to the tensile strength determined in the destructive tension tests ($f_{t,0,experimental}$). A coefficient of determination of $R^2 = 0.74$ was found. The model error is described by a normally distributed error term (Fink 2014) with the parameters $\varepsilon \sim N(\mu_\varepsilon = 0; \sigma_\varepsilon^2 = 0.018)$. Taking only the calibration data into account, the root mean square error (RMSE) of the model is 11.0, and the mean absolute percentage error (MAPE) of the model is 9.99.

In the training data set, the maximum deviation between the modelled and the experimentally determined tensile strength was found for board no. 2008 with a relative error of 43% (model: 82.8 MPa; experiment: 58.0 MPa). The predictions ($f_{t,0,estimated}$) for all other 35 boards lie within the 95% confidence interval and show a maximum deviation from the experimentally determined tensile strength ($f_{t,0,experimental}$) of $\pm 25\%$. For 22 of the 36 boards (61%), the relative error between modelled and experimentally determined tensile strength is below $\pm 10\%$ (Fig. 9).

Table 4 Regression coefficients C_i , the exponents for the dynamic modulus of elasticity^a and the tensile strength^b used in the model

	Characteristic	Symbol	Calibration interval	Value (calibrated or pre-defined ^d)	Confidence interval ^b
Parameters related to dynamic MOE (Eq. 3)	Ratio MOE parallel/perpendicular to the grain	$E_{t,0,ref}/E_{t,90,ref}$	n.a	30 ^a	n.a
	MOE exponent	a	[1; 3]	1.6	± 0.27
Parameters related to tensile strength (Eq. 4)	Tensile strength parallel to the grain	$f_{t,0,ref}$	n.a	180 MPa ^a	n.a
	Tensile strength perpendicular to the grain	$f_{t,90,ref}$	n.a	7 MPa ^a	n.a
	Tensile strength exponent	b	[1; 3]	2.5	± 0.40
Regression parameters (Eq. 5)	Intercept	C_0	[-3; 3]	1.91	± 0.29
	MOE parameter	C_1	[0; 10^{-3}]	$5.06 \cdot 10^{-5}$	$\pm 2.23 \cdot 10^{-5}$
	Tensile strength parameters	C_2	[0; 1]	0.0121	± 0.0039

The reference tensile strengths parallel ($f_{t,0,ref}$) and perpendicular to the grain ($f_{t,90,ref}$) and the ratio $E_{t,0,ref}/E_{t,90,ref}$ were assumed according to Wagenführ (2006)

^aPredefined value, based on Wagenführ (2006)

^bFor a 95% confidence, based on 36 bootstrapping-resamples

Applying the calibrated model to the (unseen) test data set reveals an even better coefficient of determination of $R^2=0.84$ (Fig. 9b). Furthermore, the root mean square error (RMSE=10.2) and the mean absolute percentage error (MAPE=9.56) are lower compared to the training data set. A maximum relative difference between the experimentally determined and the modelled tensile strength for an individual board of 20% was observed. Although, the number of boards in the test data set was small ($n=11$), these results indicate that even with unseen data the model is able to generate good estimates for the tensile strength parallel to the grain.

Comparison with models based on machine-learning techniques

The input parameters for the ML models were the two independent variables E_{dyn} and $\min(f_{t,ij})$ of each board. The density was not considered as an input parameter, since a preliminary check and the literature review indicated that the influence of this parameter on the strength of European beech wood was negligible (Table 3).

The deviation of the maximum and minimum values in the results obtained by different performance measures for each of the sixfolds for training and validating was very limited, indicating that all machine-learning models showed no tendency towards under- or overfitting (Table 5). Overfitting would mean that the analysis would correspond too closely to this particular set of data, without being able to predict subsequent (unseen) observations reliably. Theoretically, the prediction model

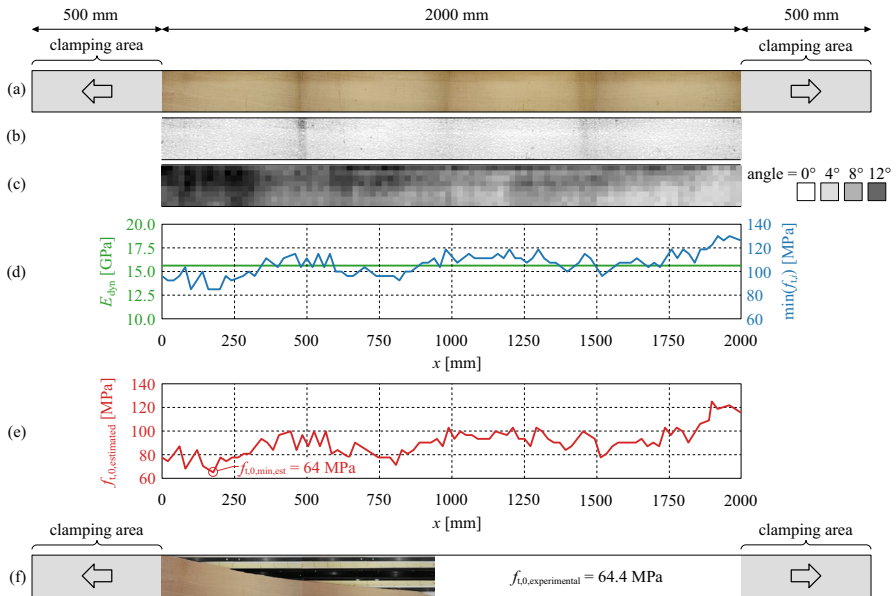


Fig. 8 Overview of all steps of the reference model using the example of board no. 1035: photos of the board segments between the clamping jaws (a); post-processed black-and-white image of the medullary ray spindles (b); matrix of local fibre directions (c). Based on the measured E_{dyn} and $\min(f_{t,ij})$ along the board's longitudinal axis (d), the tensile strength $f_{t,0,\text{estimated}}$ is predicted (e). The fracture pattern (f) agrees well with the estimated fibre direction. The modelled ($f_{t,0,\text{estimated}} = 64$ MPa) and experimentally determined tensile strength ($f_{t,0,\text{experimental}} = 64.4$ MPa) are on a similar level and failure occurred in the area of maximum fibre inclination

works best when R^2 equals one and both RMSE and MAPE equal zero. Table 5 summarises the performance values R^2 , RMSE and MAPE of the five models for the test data set, which was not considered in all prior analyses and therefore called 'unseen' in order to determine the generalisation ability of the models.

The results clearly show that the predictions of all machine-learning algorithms, according to the relevant indices (R^2 , RMSE, MAPE), are highly correlated with the experimental observations of the mechanical tensile strength property (Table 5). When applied to the test data set, the predictive models support-vector machine ($R^2 = 0.87/\text{RMSE} = 8.40/\text{MAPE} = 7.72\%$) and random forest ($R^2 = 0.88/\text{RMSE} = 8.16/\text{MAPE} = 8.48\%$) perform best, i.e. the predicted values were closest to the experimentally determined tensile strengths. The artificial neural network model ($R^2 = 0.86/\text{RMSE} = 8.46/\text{MAPE} = 7.59\%$) showed a similar prediction quality and performed best with regard to the MAPE. Even the worst performance of the machine-learning algorithms (Decision Tree algorithm) had acceptable accuracy indices of $R^2 = 0.81$, $\text{RMSE} = 9.73$ and $\text{MAPE} = 9.91$ for the test data set.

Due to the small dataset, the investigations were limited to the evaluation of the applicability of specific machine-learning techniques. The use of deep learning approaches, which require very large data sets and are computationally intensive, was not possible. This study shows that the reference model as well as shallow machine-learning algorithms can be used to analyse the limited dataset and

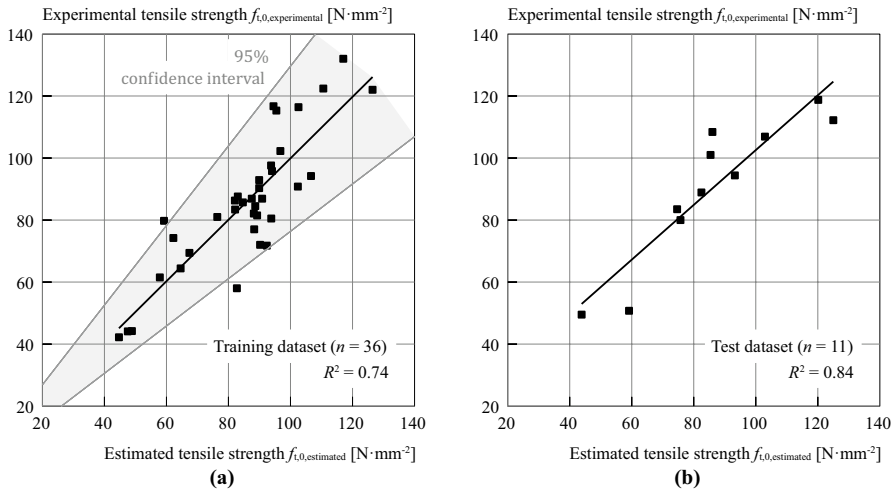


Fig. 9 Correlation analysis between the modelled tensile strength $f_{t,0,estimated}$ and the experimentally determined tensile strength $f_{t,0,experimental}$ for the training data set **(a)** ($n=36$; $R^2=0.74$) and the test data set **(b)** ($n=11$; $R^2=0.84$)

to predict the tensile strength parallel to the grain of European beech boards with high accuracy. However, the use of shallow machine-learning algorithms on a small dataset required the use of cross-validation methods and hold-out tests (Varma and Simon 2006). As discussed above, efficient strength grading of timber is important when attempting at controlling the inherent heterogeneous material structure on different scales and the high variability of wood properties. Machine learning is a powerful tool in this respect and can help to overcome the recurring challenge in wood technology to transform the very heterogeneous raw material wood into products with high value and well-defined properties (Schubert et al. 2020; Schubert and Kläusler 2020).

Conclusion

The present study explores the potential of using information on the local fibre direction in addition to the dynamic modulus of elasticity in the strength grading process of European beech (*Fagus sylvatica* L.) boards. Based on investigations on 36 knot-free boards assigned to a training or calibration data set, which were used to train different machine-learning techniques (Support-Vector machines, Decision Tree, Random Forest, and Artificial Neural Network using a 6-k cross-validation approach), and another 11 boards assigned to the ‘unseen’ test data set, the following conclusions can be drawn:

- Data on the local fibre direction are very important for understanding and predicting the tensile strength parallel to the grain of European beech timber. Espe-

Table 5 Descriptive statistics for the training/validation data set (6-k cross-validation) and the test data set

Model	Training/validation data set			Test data set		
	R^2	RMSE	MAPE ^g	R^2	RMSE	MAPE
Reference model	0.74	11.0	9.99	0.84	10.2	9.56
Support-vector machine ^c	0.71 ^a ± 0.07 ^b	11.5 ± 1.68	10.2 ± 2.15	0.87	8.40	7.72
Decision tree ^d	0.83 ± 0.22	8.99 ± 2.86	7.79 ± 3.71	0.81	9.73	9.91
Random forest ^e	0.87 ± 0.13	8.19 ± 2.30	7.13 ± 2.39	0.88	8.16	8.48
Artificial neural network ^f	0.72 ± 0.07	11.4 ± 1.89	10.2 ± 2.75	0.86	8.46	7.59

^aSelected model

^bStandard deviation of the 6-k cross-validation

^cMATLAB parameters: ‘KernelFunction’: linear; ‘KernelScale’: 2.18; ‘IterationLimit’: 1e6; ‘Solver’: SMO; ‘BoxConstraint’: 12.635

^dMATLAB parameters: ‘MinParent’: 10; ‘MinLeaf’: 1; ‘MaxSplits’: 29; ‘PruneCriterion’: mse; ‘PredictorSelection’: allsplit

^eMATLAB parameters: ‘Trees’: 1000; ‘mtry’: 2/3; ‘Sample size’: size (Xtrain, 1); ‘Splitting rule’: Randomly selected mtry; ‘MinLeafSize’: 2; ‘NumPredictorsToSample’: 2

^fMATLAB parameters: ‘Architecture’: 36-[5]-1; ‘Training algorithm’: Bayesian regularisation backpropagation; ‘Transfer function’: tansig (hidden layer), purelin (output layer); ‘Epochs’:5; ‘Learning rate’: 0.01.

^gInterpretation of the mean absolute percentage error (MAPE) according to Lewis (1982): MAPE ≤ 10% ↔ high accuracy prediction, 10% < MAPE ≤ 20% ↔ good prediction, 20% < MAPE ≤ 50% ↔ reasonable prediction, > 50% ↔ inaccurate prediction.

cially for knot-free boards, this is considered the key parameter to achieve predictions of high accuracy.

- A model that takes into account the dynamic modulus of elasticity and a second parameter representing the critical local fibre direction was developed using a training data set (77% of the data). For this training data set, a coefficient of determination of $R^2=0.74$ between the predicted tensile strength and the experimentally determined tensile strength parallel to the grain and a mean absolute percentage error (MAPE) of 9.99% was found. Applying the model to the unseen test data set (23% of the data) showed an even better coefficient of determination of $R^2=0.84$ and a lower MAPE of 9.56%.
- Shallow machine-learning algorithms in combination with cross-validation methods were successfully used to further improve the prediction accuracy. The machine-learning techniques support-vector machine ($R^2=0.87$ /RMSE=8.40/MAPE=7.7%) and random forest ($R^2=0.88$ /RMSE=8.16/MAPE=8.5%) showed the best performance when applied to the unseen test data set.

The outcomes of this study indicate that the application of combined approaches, including experimental methods and machine-learning, has a great potential for increasing the precision of the strength grading of European beech timber. However, due to the limited size of the dataset available for this study, applying the presented methods to a larger dataset would be important and is envisaged in the course of follow-up projects. In the future, such combined approaches have the potential to

contribute to a more resource-efficient use of this timber species widely available in Central Europe and may open new and more demanding fields for high-level timber applications.

Author contributions All authors contributed to the study conception and design. Material preparation, data collection and analysis were performed by TE, PP and MS. The first draft of the manuscript was written by TE, PP, and MS, and all authors contributed to the following versions of the manuscript. All authors read and approved the final manuscript.

Funding The authors wish to acknowledge the support of the Swiss Federal Office for the Environment FOEN within the framework of the Aktionsplan Holz [Projekt REF-1011-04200].

Availability of data and material In order to allow for transparency, verifiability and suggestions for further improvement of the presented methods, the following data will be made available for all 47 boards included in the study: Original images, processed images showing the identified medullary ray spindles, matrices of the local fibre directions, a table including information on the density, the dynamic and static MOE and the tensile strength parallel to the grain.

Declarations

Conflict of interest On behalf of all authors, the corresponding author states that there is no conflict of interest and that there are no competing interests.

Consent to publication Consent to publication has been received explicitly from all authors, as well as from the responsible authorities at the institutes where the work has been carried out.

Consent to participate Consent to participate has been received explicitly from all co-authors.

References

- Aicher S, Höfflin L, Behrens W (2001) A study on tension strength of finger joints in beech wood laminations. *Otto Graf J* 12:169–186
- Ashby MF, Easterling KE, Harrysson R, Maiti SK (1985) The fracture and toughness of woods. *Proc R Soc London Ser A Math Phys Sci* 398: 261–280. <https://doi.org/10.1098/rspa.1985.0034>
- Baradit E, Aedo R, Correa J (2006) Knots detection in wood using microwaves. *Wood Sci Technol* 40(2):118–123. <https://doi.org/10.1007/s00226-005-0027-8>
- Belkacemi M, Massich J, Lemaitre G, Stolz C, Daval V, Pot G, Aubreton O, Collet R, Meriaudeau F (2016) Wood fiber orientation assessment based on punctual laser beam excitation: a preliminary study. In: *Proceedings of the 2016 international conference on quantitative infrared thermography (QIRT)*, Gdansk, Poland
- Besseau B, Pot G, Collet R, Viguier J (2020) Influence of wood anatomy on fiber orientation measurement obtained by laser scanning on five European species. *J Wood Sci* 66(1):1–12. <https://doi.org/10.1186/s10086-020-01922-y>
- Bishop CM (2006) *Pattern recognition and machine learning*. Springer-Verlag, Information Science and Statistics
- Blaß HJ, Denzler J, Frese M, Glos P, Linsenmann P (2005) *Biegefestigkeit von Brettschichtholz aus Buche*. Karlsruhe Berichte zum Ingenieurholzbau—Band 1. Universitätsverlag Karlsruhe
- Brandner R, Schickhofer G (2008) Glued laminated timber in bending: New aspects concerning modelling. *Wood Sci Technol* 42:401–425. <https://doi.org/10.1007/s00226-008-0189-2>
- Brännström M, Manninen J, Oja J (2008) Predicting the strength of sawn wood by tracheid laser scattering. *BioResources* 3(2):437–451
- Breiman L (2001) Random forests. *Mach Learn* 45:5–32. <https://doi.org/10.1023/A:1010933404324>

- Briggert A, Olsson A, Oscarsson J (2016) Three-dimensional modelling of knots and pith location in Norway spruce boards using tracheid-effect scanning. *Eur J Wood Prod* 74(5):725–739. <https://doi.org/10.1007/s00107-016-1049-7>
- Cramer SM, McDonald KA (1989) Predicting lumber tensile stiffness and strength with local grain angle measurements and failure analysis. *Wood Fiber Sci* 21(1):393–410
- Curti R, Marcon B, Denaud L, Collet R (2018) Effect of grain direction on cutting forces and chip geometry during green beech wood machining. *BioResources* 13(3):5491–5503
- Daval V, Pot G, Belkacemi M, Meriaudeau F, Collet R (2015) Automatic measurement of wood fiber orientation and knot detection using an optical system based on heating conduction. *Opt Express* 23(26):33529–33539. <https://doi.org/10.1364/OE.23.033529>
- Denzler JK, Weidenhiller A (2015) Microwave scanning as an additional grading principle for sawn timber. *Eur J Wood Wood Prod* 73(4):423–431. <https://doi.org/10.1007/s00107-015-0906-0>
- DIN 4074-5 (2008) Strength grading of wood—Part 5—Sawn hardwood. DIN
- DIN 4074-1 (2012) Strength grading of wood—Part 1—Coniferous sawn timber. DIN
- DIN EN 408 (2012) Timber structures—Structural timber and glued laminated timber—Determination of some physical and mechanical properties. CEN
- Ehlbeck J, Colling F, Görlacher R (1985) Einfluss keilgezinkter Lamellen auf die Biegefestigkeit von Brettschichtholzträgern (Influence of finger-jointed laminations on the bending strength of glued laminated timber beams) (In German). *Holz Roh Werkst* 43:333–337. <https://doi.org/10.1007/BF02607817>
- Ehrhart T (2019) European beech glued laminated timber. PhD Thesis Nr. 26173. ETH Zürich. <https://doi.org/10.3929/ethz-b-000402805>
- Ehrhart T, Fink G, Steiger R, Frangi A (2016a) Experimental investigation of tensile strength and stiffness indicators regarding European beech timber. In: World conference on timber engineering. Vienna, Austria
- Ehrhart T, Fink G, Steiger R, Frangi A (2016b) Strength grading of European beech lamellas for the production of GLT and CLT. International Network on Timber Engineering Research, Meeting 49. Paper 49-5-1. Graz, Austria
- Ehrhart T, Steiger R, Frangi A (2018a) A non-contact method for the determination of fibre direction of European beech wood (*Fagus sylvatica* L.). *Eur J Wood Prod* 76(3):925–935. <https://doi.org/10.1007/s00107-017-1279-3>
- Ehrhart T, Steiger R, Palma P, Frangi A (2018b) Estimation of the tensile strength of European beech timber boards based on density, dynamic modulus of elasticity and local fibre orientation. In: World conference on timber engineering (WCTE 2018), Seoul, Republic of Korea
- Fathi H, Nasir V, Kazemirad S (2020) Prediction of the mechanical properties of wood using guided wave propagation and machine learning. *Constr Build Mater*. <https://doi.org/10.1016/j.conbuildmat.2020.120848>
- Federal Office for the Environment FOEN (2018) Swiss statistical yearbook of forestry (Jahrbuch Wald und Holz—Annuaire La forêt et le bois). UZ Nr. 1830, FOEN, Bern, Switzerland (in German and French)
- Fink G (2014) Influence of varying material properties on the load-bearing capacity of glued laminated timber. PhD Thesis Nr. 21746. ETH Zürich. <https://doi.org/10.3929/ethz-a-010108864>
- Foley C (2001) A three-dimensional paradigm of fiber orientation in timber. *Wood Sci Technol* 35(5):453–465. <https://doi.org/10.1007/s002260100112>
- Frese M (2006) Bending strength of beech glued laminated timber (in German). PhD Thesis. Universität Karlsruhe, Germany
- Frühwald K, Schickhofer G (2005) Strength grading of hardwoods. In: Proceedings of the 14th international symposium on nondestructive testing of wood. Hannover, Germany, pp 198–208
- Frühwald A, Ressel JB, Bernasconi A, Becker P, Pitzner B, Wonnemann R, Mantau U, Sörgel C, Thoroe C, Dieter M, Englert H (2003). Hochwertiges Brettschichtholz aus Buchenholz. Forschungsprojekt—Abschlussbericht (High-quality glued laminated timber made of beech wood. Research project—Final report) (in German). Bundesforschungsanstalt für Forst- und Holzwirtschaft, Hamburg, Germany
- Glos P, Lederer B (2000) Sortierung von Buchen- und Eichenschnittholz nach der Tragfähigkeit und Bestimmung der zugehörigen Festigkeits- und Steifigkeitskennwerte (Sorting of beech and oak sawn timber according to the load-bearing capacity and determination of the associated strength and stiffness properties) (in German). TU München, Holzforschung München (internal report no. 98508), Munich, Germany

- Hankinson RL (1921) Investigation of crushing strength of spruce at varying angles of grain. Air Force Information Circular No. 259, U. S. Air Service
- Hinton GE, Salakhutdinov RR (2006) Reducing the dimensionality of data with Neural Networks. *Science* 313:504–507. <https://doi.org/10.1126/science.1127647>
- Hübner U (2013) Mechanische Kenngrößen von Buchen-, Eschen- und Robinienholz für lastabtragende Bauteile (Mechanical properties of beech, ash and black locust wood for load-carrying members) (in German). PhD Thesis. Graz University of Technology. <https://doi.org/10.3217/978-3-85125-314-6>
- JCSS (2006) JCSS Probabilistic model code. Part III—Resistance models. Properties of timber. In: JCSS probabilistic model code. Joint committee on structural safety, p 16
- Jungo N (2016) Investigations on indicating parameters for the strength properties of beech wood (in German). Master Project Thesis. ETH Zürich
- Kohavi R (1995) A study of cross-validation and bootstrap for accuracy estimation and model selection. In: Proceedings of the 14th international joint conference on artificial intelligence, vol 21995, pp 1137–1143. Morgan Kaufmann Publishers Inc.: Montreal, Quebec, Canada
- Kotsiantis SB (2013) Decision trees: a recent overview. *Artif Intell Rev* 39:261–283. <https://doi.org/10.1007/s10462-011-9272-4>
- Krapez JC, Gardette G, Balageas DL (1996) Thermal ellipsometry in steady-state and by lock-in thermography: application to anisotropic materials characterization. In: Proceedings of quantitative infrared thermography QIRT 96 eurotherm seminar, vol 50, pp 257–62. <https://doi.org/10.21611/qirt.1996.042>
- LeCun Y, Bengio Y, Hinton G (2015) Deep learning. *Nature* 521:436–444. <https://doi.org/10.1038/nature14539>
- Lewis CD (1982) Industrial and business forecasting methods. Butterworths, London, UK. <https://doi.org/10.1002/for.3980020210>
- Lukacevic M, Füssl J (2014) Numerical simulation tool for wooden boards with a physically based approach to identify structural failure. *Eur J Wood Prod* 72(4):497–508. <https://doi.org/10.1007/s00107-014-0803-y>
- Mansfield SD, Iliadis L, Avramidis S (2007) Neural network prediction of bending strength and stiffness in western hemlock (*Tsuga heterophylla* Raf.). *Holzforschung* 61:707–716. <https://doi.org/10.1515/HF.2007.115>
- Matthews PC, Beech BH (1976) US Patent 3,976,384: method and apparatus for detecting timber defects
- Matthews PC, Soest JF (1986) US Patent 4,606,64: method for determining localized fiber angle in a three dimensional fibrous material
- Metcalfe L, Dashner B (2002) US Patent 2002/0025061A1: high speed and reliable determination of lumber quality using grain influenced distortion effects
- Norimoto M, Yamada T (1972) The dielectric properties of wood VI: On the dielectric properties of the chemical constituents of wood and the dielectric anisotropy of wood. *Wood Res Bull Wood Res Inst Kyoto Univ* 52: 31–43. <http://hdl.handle.net/2433/53414>
- Norton JAP, McLaughlan TA, Kusec DJ (1974) US Patent 3,805,156: wood slope of grain indicator
- Nyström J (2003) Automatic measurement of fiber orientation in softwoods by using the tracheid effect. *Comput Electron Agric* 41(1–3):91–99. [https://doi.org/10.1016/S0168-1699\(03\)00045-0](https://doi.org/10.1016/S0168-1699(03)00045-0)
- Ohnesorge D, Richter K, Becker G (2010) Influence of wood properties and bonding parameters on bond durability of European Beech (*Fagus sylvatica* L.) glulams. *Ann for Sci* 67:601. <https://doi.org/10.1051/forest/2010002>
- Olsson A, Oscarsson J (2017) Strength grading based on high resolution laser scanning and dynamic excitation: a full scale investigation of performance. *Eur J Wood Prod* 75(1):17–31. <https://doi.org/10.1007/s00107-016-1102-6>
- Olsson A, Oscarsson J, Serrano E, Källsner B, Johansson M, Enquist B (2013) Prediction of timber bending strength and in-member cross-sectional stiffness variation on the basis of local wood fibre orientation. *Eur J Wood Prod* 71(3):319–333. <https://doi.org/10.1007/s00107-013-0684-5>
- Olsson A, Pot G, Viguier J, Faydi Y, Oscarsson J (2018) Performance of strength grading methods based on fibre orientation and axial resonance frequency applied to Norway spruce (*Picea abies* L.), Douglas fir (*Pseudotsuga menziesii* (Mirb.) Franco) and European oak (*Quercus petraea* (Matt.) Liebl./*Quercus robur* L.). *Ann for Sci* 75(4):1–18. <https://doi.org/10.1007/s13595-018-0781-z>
- Plos M, Fortuna B, Straze A, Turk G (2018) Visual grading of beech wood—a decision tree approach. In: World conference on timber engineering. Seoul, Republic of Korea
- Ridley-Ellis D, Stapel P, Baño V (2016) Strength grading of sawn timber in Europe: an explanation for engineers and researchers. *Eur J Wood Prod* 74:291–306. <https://doi.org/10.1007/s00107-016-1034-1>

- Sarén MP, Serimaa R, Tolonen Y (2006) Determination of fiber orientation in Norway Spruce using X-ray diffraction and laser scattering. *Eur J Wood Prod* 64(3):183–188. <https://doi.org/10.1007/s00107-005-0076-6>
- Sarnaghi AK, van de Kuilen JWG (2019) Strength prediction of timber boards using 3D FE-analysis. *Constr Build Mater* 202:563–573. <https://doi.org/10.1016/j.conbuildmat.2019.01.032>
- Sauter UH, Breinig L (2016) European hardwoods for the building sector: reality of today—Possibilities for tomorrow, WP 1-Hardwood resources in Europe: standing stock and resource forecasts. Workshop Garmisch-Partenkirchen, Germany
- Schindelin J, Arganda-Carreras I, Frise E, Kaynig V, Longair M, Pietzsch T, Preibisch S, Rueden C, Saalfeld S, Schmid B, Tinevez JY, White DJ, Hartenstein V, Eliceiri K, Tomancak P, Cardona A (2012) Fiji: an open-source platform for biological-image analysis. *Nat Methods* 9(7):676–682. <https://doi.org/10.1038/nmeth.2019>
- Schlotzhauer P, Wilhelms F, Lux C, Bollmus S (2018) Comparison of three systems for automatic grain angle determination on European hardwood for construction use. *Eur J Wood Prod* 76(3):911–923. <https://doi.org/10.1007/s00107-018-1286-z>
- Schubert M, Kläusler O (2020) Applying machine learning to predict the tensile shear strength of bonded beech wood as a function of the composition of polyurethane prepolymers and various pretreatments. *Wood Sci Technol* 54:19–29. <https://doi.org/10.1007/s00226-019-01144-6>
- Schubert M, Luković M, Christen H (2020) Prediction of mechanical properties of wood fiber insulation boards as a function of machine and process parameters by random forest. *Wood Sci Technol* 54:703–713. <https://doi.org/10.1007/s00226-020-01184-3>
- Simonaho SP, Palviainen J, Tolonen Y, Silvennoinen R (2004) Determination of wood grain direction from laser light scattering pattern. *Opt Lasers Eng* 41(1):95–103. [https://doi.org/10.1016/S0143-8166\(02\)00144-6](https://doi.org/10.1016/S0143-8166(02)00144-6)
- Snoek J, Larochelle H, Adams RP (2012) Practical Bayesian optimization of machine learning algorithms. In: Proceedings of the 25th international conference on neural information processing systems, vol 2. Curran Associates Inc.: Lake Tahoe, Nevada. pp 2951–2959
- Soest JF (1997) US Patent 5,703,960: lumber defect scanning including multi-dimensional pattern recognition
- Steele PH, Neal SC, McDonald SM (1991) The slope-of-grain indicator for defect detection in unplanned hardwood lumber. *For Prod J* 41(1):15–20
- Vapnik VN (1995) The nature of statistical learning theory. Springer-Verlag. <https://doi.org/10.1007/978-1-4757-3264-1>
- Varma S, Simon R (2006) Bias in error estimation when using cross-validation for model selection. *BMC Bioinform* 7:91. <https://doi.org/10.1186/1471-2105-7-91>
- Viguier J, Jehl A, Collet R, Bleron L, Meriaudeau F (2015) Improving strength grading of timber by grain angle measurement and mechanical modeling. *Wood Mat Sci Eng* 10(1):145–156. <https://doi.org/10.1080/17480272.2014.951071>
- Viguier J, Bourreau D, Bocquet JF, Pot G, Bléron L, Lanvin JD (2017) Modelling mechanical properties of Spruce and Douglas Fir timber by means of X-ray and grain angle measurements for strength grading purpose. *Eur J Wood Prod* 75(4):527–541. <https://doi.org/10.1007/s00107-016-1149-4>
- Viguier J, Bourgeay C, Rohumaa A, Pot G, Denaud L (2018) An innovative method based on grain angle measurement to sort veneer and predict mechanical properties of beech laminated veneer lumber. *Constr Build Mater* 181:146–155. <https://doi.org/10.1016/j.conbuildmat.2018.06.050>
- Wagenführ R (2006) *Holzatlas* (in German), 6th edn. Carl Hanser Verlag, Dresden, Germany
- Weidenhiller A, Linsenmann P, Lux C, Brüchert F (2019) Potential of microwave scanning for determining density and tension strength of four European hardwood species. *Eur J Wood Prod* 77(2):235–247. <https://doi.org/10.1007/s00107-019-01387-x>
- Westermayr M, Stapel P, Van de Kuilen JWG (2018) Tensile and compression strength of small cross section beech glulam members. International Network on Timber Engineering Research, Meeting 51. Paper 51-12-2. Tallinn, Estonia

Publisher's Note Springer Nature remains neutral with regard to jurisdictional claims in published maps and institutional affiliations.